sustainability

MDPI

Communication

Development of a Portable and Sensitive CO_2 Measurement Device with NDIR Sensor Clusters and Minimizing Water Vapor Impact

Zhentao Wu [1], Xiaobing Pang [1,*], Bo Xing [2], Qianqian Shang [1], Hai Wu [3,*], Yu Lu [1], Haonan Wu [1], Yan Lyu [1], Jingjing Li [2], Baozhen Wang [4], Shimin Ding [4], Dongzhi Chen [5] and Jianmeng Chen [1]

1 College of Environment, Zhejiang University of Technology, Hangzhou 310014, China
2 Shaoxing Ecological and Environmental Monitoring Center of Zhejiang Province, Shaoxing 312000, China
3 National Institute of Metrology, Beijing 102200, China
4 Green Intelligence Environmental School, Yangtze Normal University, Chongqing 408100, China
5 School of Petrochemical Engineering & Environment, Zhejiang Ocean University, Zhoushan 316022, China
* Correspondence: pangxb@zjut.edu.cn (X.P.); wuhai@nim.ac.cn (H.W.)

Abstract: Increasing carbon dioxide (CO_2) concentrations threaten human production and life. Currently the equipment used for CO_2 monitoring is heavy and expensive, without a portable CO_2 detector that is inexpensive and resistant to interference. Here we designed a portable CO_2 detector based on no-dispersive infrared sensors to measure CO_2 concentration. The detector, which has a mass of 1 kg, is powered by a lithium battery with dimensions of 200 mm (length) × 150 mm (width) × 100 mm (height). Considering the fact that field observations are susceptible to humidity, a series of experiments were carried out to reduce the humidity interference on sensor responses at a laboratory. The values of humidity and CO_2 variation were used in a regression model analysis to determine a quadratic function with an R^2 above 0.94. The detector was compared with a reference analyzer in ambient CO_2 measurement during a 7-day field campaign in Hangzhou, China. After humidity correction, the data show better correlation with the reference data, with the R^2 0.62–0.97 increasing from 0.62–0.97 compared to before the correction and the value deviation decreasing to less than 3%. Cluster analysis of sensors revealed a reduction in average relative deviation of up to 1.4% as the number of sensors increased.

Keywords: CO_2 measurement device; humidity interference; non-dispersive infrared (NDIR); clustering sensors; regression model

check for updates

Citation: Wu, Z.; Pang, X.; Xing, B.; Shang, Q.; Wu, H.; Lu, Y.; Wu, H.; Lyu, Y.; Li, J.; Wang, B.; et al. Development of a Portable and Sensitive CO_2 Measurement Device with NDIR Sensor Clusters and Minimizing Water Vapor Impact. *Sustainability* **2023**, *15*, 1533. https://doi.org/10.3390/su15021533

Academic Editor: Adam Smoliński

Received: 14 November 2022
Revised: 21 December 2022
Accepted: 5 January 2023
Published: 12 January 2023

1. Introduction

Carbon dioxide (CO_2) is a major greenhouse gas, the concentration of which has been rising every year since industrial revolution, causing global climate change [1,2]. Monitoring the level of CO_2 in the environment is important for mitigating the greenhouse effect [3]. In early days, flask-based measurements required observers to collect samples, which were then transported to a laboratory for analysis with gas chromatographs [4]. Such detection methods carried a lag in data that made it difficult to capture the dynamic changes in CO_2 concentration.

Optical detection technology can provide great advantages with regards to gas selectivity, accuracy and sensitivity. As a result, it is widely used for environmental CO_2 detection [5,6]. To address global-scale monitoring requirements, probing satellites with spectroscopic techniques have been deployed into space to monitor atmospheric CO_2 concentrations [7–9]. This method has obvious disadvantages including high cost, low resolution and large uncertainty. With the development of laser spectroscopy technology, a number of continuous measurement CO_2 instruments have been developed for CO_2

monitoring based on highly accurate detection techniques such as cavity ring-down spectroscopy (CRDS) [10], off-axis integrated cavity output spectroscopy [11] and tunable diode laser absorption spectroscopy [12]. The source-sink of CO_2 and climate effects in the environment were revealed by these high-precision analytical devices in CO_2 networks over the world [13–16]. Due to the cost of the networks, it is difficult to develop them on a large scale with a higher spatial density of observations. Meanwhile the majority of such instruments are large and complex to operate, as well as requiring strict environmental conditions at the measurement site. Therefore, they are not suitable for use in field observation experiments where conditions are complex.

Electrochemical sensors as a conventional detection technology are widely used in environmental air quality monitoring for the rapid assessment of regional environmental pollution levels. Some rare earth elements were added to the electrodes for electrochemical CO_2 sensors, making the sensors more expensive [17]. In addition, most electrochemical sensors need to be pre-heated for a long time in order to reach a suitable operating temperature [18]. Compared to optical detection techniques these sensors have a longer response time, usually exceeding 60 s [19]. With the advent of widely available and low-cost mid-infrared light sources and detectors, one optical absorption method called no-dispersive infrared (NDIR) technique was applied for the development of miniature CO_2 sensors. A chamber-less NDIR gas sensor was developed with low robustness using a light source with an embedded parabolic reflector [20]. A multiplexed NDIR gas sensing platform was designed for CO_2 measurement with a 2 ppm detection limit [21]. A miniaturized NDIR CO_2 sensor was implemented on a silicon chip consisting of a hollow metallic cylindrical cavity along with access waveguides showing a limit of detection of roughly 100 ppm [22]. Nevertheless, the response of the sensor is still susceptible to drift-induced variations in the ambient air.

Variations in atmospheric pressure can affect the gas volume in the chamber of the sensor causing a corresponding measurement error. A study has reported that the root–mean–square error of a, NDIR sensor was 2.1 ppm when pressure changed over 45,000 Pa [23]. However, such a large fluctuation in atmospheric pressure is not expected in ambient air testing in the field. Gas molecule diffusion within the detection chamber is affected by temperature, and the absorption peaks of water molecules overlapped with $CO_{2,}$ affecting detection accuracy [24,25]. Therefore, temperature and humidity are two major ambient parameters that influence CO_2 gas measurement in applications [26,27]. The effects of both on NDIR sensors have been evaluated in some studies. The long term-stability of a fully integrated NDIR CO_2 sensor on a silicon chip was subject to the temperature fluctuations in the laboratory [28]. The NDIR sensors respond linearly to CO_2 when measuring calibration tanks, but the regression slope between measured and assigned CO_2 differs between individual sensors and was influenced by meteorological conditions, especially relative humidity (RH) [29]. Currently some desiccants are used to eliminate the interference of humidity with the detection. Therefore, there are few correction methods for RH in the literature. Understanding atmospheric CO_2 variations is a long-term effort, however, and a regular desiccant replacement would significantly increase the human cost of monitoring. Hence, the reliability of the CO_2 sensor needs to be addressed, given these environmental restrictions.

In this study, a portable CO_2 measurement device was designed by six NDIR sensors for ambient CO_2 monitoring. The effect of humidity on the signal drift of the sensor was studied by simulating real atmospheric conditions at laboratory. The CO_2 device was deployed for measure ambient air with a reference analyzer in a 7-day field campaign. Using regression models, we obtained correction equations for humidity and CO_2 variation values correcting the data of the CO_2 device with the reference analyzer to eliminate ambient humidity interference. Detection accuracy was further improved by clustering sensors as well as limiting the effects of inter-sensor variability.

2. Materials and Methods

2.1. Self-Developed CO_2 Device

The self-developed CO_2 device is shown in a red rectangle (Figure 1). NDIR optical CO_2 sensors (K30, SenseAir, Delsbo, Sweden) were integrated into the left and right of the device (three on each side), the dimensions of which were 57 mm (length) × 48 mm (width) × 8 mm (height). Gas diffusion sampling is used to detect calibration gas or sampling air directly in contact with the sensor surface membrane, and the corresponding voltage signal is detected by an internal photoelectric element. In addition, the surface membrane has a filtering effect on particulate matter so that no individual flow cell device is required. The sensor internal light intensity is attenuated by the diffusion of CO_2 from air onto the sensor surface, and the CO_2 concentration is measured according to the intensity of the attenuation. An LM35 temperature sensor (Texas Instruments, Dallas, TX, USA) and an HIH-3610 humidity probe (Honeywell, Charlotte, NC, USA) were employed to measure ambient air temperature and RH. A 20,000 mAh lithium battery was fitted inside the device to power the sensors and microcomputer. The dimensions of the whole device were 200 mm (length) × 150 mm (width) × 100 mm (height) and its weight was 1 kg.

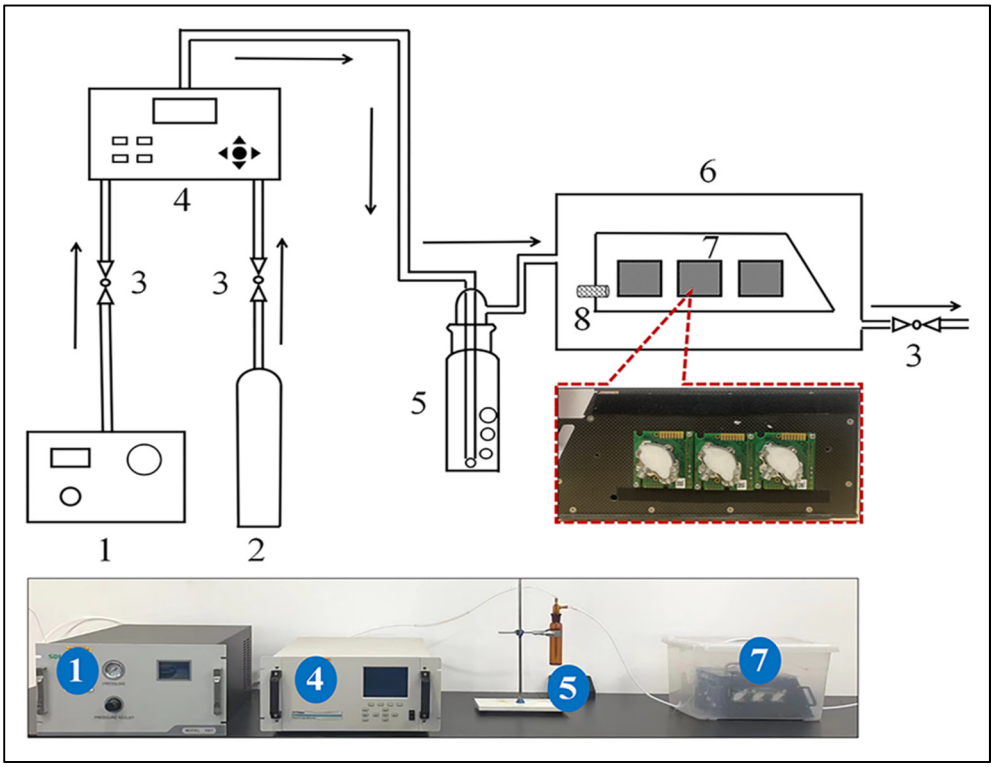

Figure 1. Schematic and actual diagram of a humidity interference experiment with a self-developed CO_2 device. The experimental devices are labeled with numbers and presented below the diagram (1—Pure air generator, 2—CO_2 standard gas, 3—Valve, 4—Gas dilution device, 5—Bubble absorption bottle, 6—Acrylic box, 7—CO_2 sensors and 8—Temperature and humidity sensor). The direction of airflow is represented by black arrows. The details of the CO_2 device are shown in the red rectangle with three CO_2 sensors on left and right side (sensor 1#–6#).

2.2. Data Acquisition

All sensor boards with a time resolution of 2 s were connected through a Smacq data-acquisition (DAQ) device (USB-3200, Smacq Corporation, Beijing, China) to our in-house designed LabVIEW DAQ software (LabVIEW 2012, National Instrument, Austin, TX, USA). The signal voltages of the sensors were monitored and recorded in the software. The voltage signals were converted into their parameter units including gas mixing ratio (ppm), RH (%) and temperature (°C) in the software. The system was controlled by a microcomputer

with Windows 10, which showed and saved data. The microcomputer was equipped with an inter processor with 64 GB of memory, and was powered by a lithium battery with dimensions of 12 mm (length) × 11 mm (width) × 40 mm (height).

2.3. Interference from Humidity

In this study the influence of humidity on the CO_2 sensors was initially investigated through testing the variations of the sensor in clean 'zero air' at different controlled RH (0%, 35%, 50%, 65%, and 80%). 'Zero air' is defined as clean air free from water vapor, particulate matter and other gases such as sulphur dioxide, ozone, carbon monoxide and so on. The schematic diagram of a humidity interference experiment with a self-developed CO_2 device is shown in Figure 1. A pure air generator (Model 1001, Beijing SDL Technology Corporation, Beijing, China) was used to create the initially dry zero air in this experiment. The zero gas generator and CO_2 standard gas were connected to a gas dilution device (T1700H, Beijing SDL Technology Corporation, China) together with valves. The humidity of zero gas was controlled by adjusting the flow rate of the gas dilution device and the volume of steam water in the bubble absorption bottle to achieve the target value. The specific experimental parameters are shown in Table 1. The self-developed CO_2 device was placed in a sealed acrylic chamber with a one-way valve at the end of the chamber to control exhaust gas. Humidified zero air or CO_2 standard gas were detected by the CO_2 sensors and the humidity sensor of the CO_2 device at the chamber. The stable data from the device were selected for analysis of the interference of humidity with detection performance, as described in Figure 2.

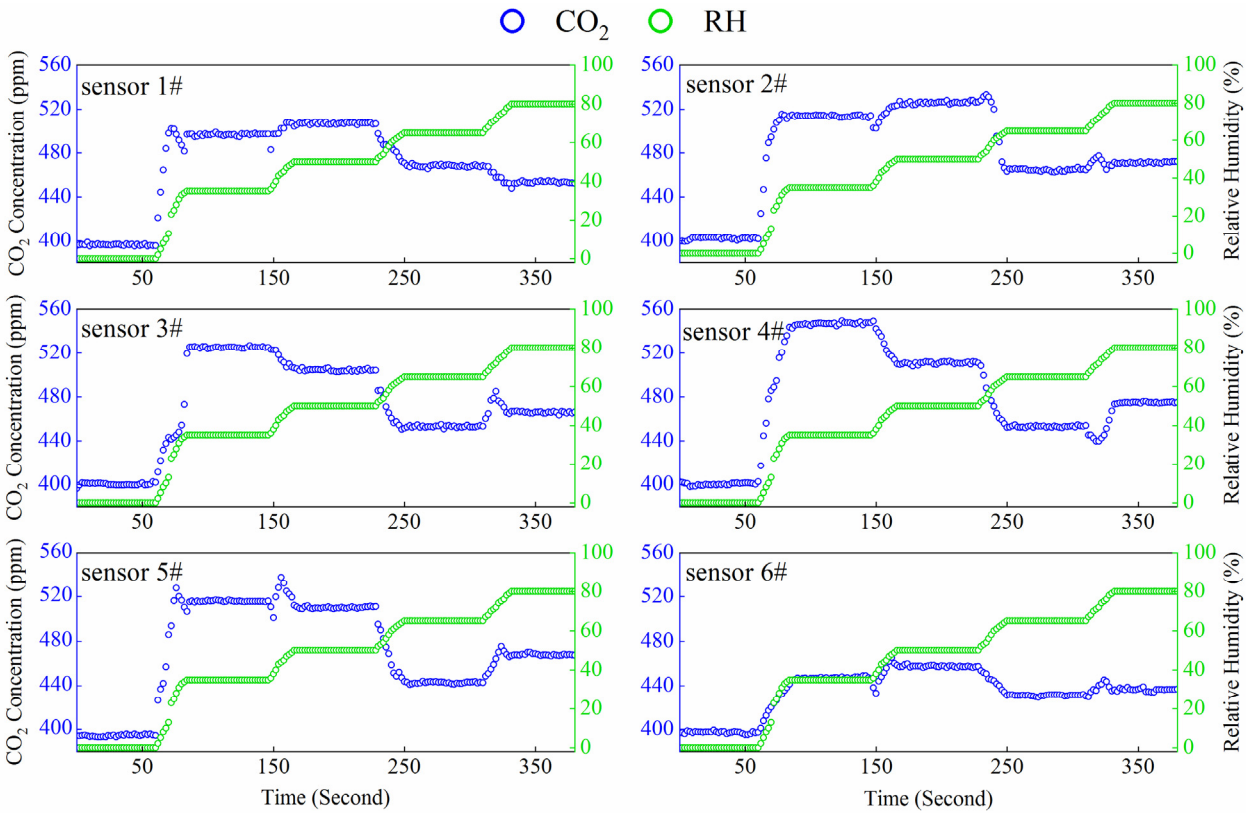

Figure 2. Humidity effects on CO_2 concentration for the six CO_2 sensors with zero air at laboratory. The CO_2 device stabilization time varies from 20–40 s, with the horizontal phase being a steady state maintenance of one minute.

Table 1. Operating parameters of the humidity interference experimental devices. The flow rate is adjusted by the gas dilution device and the water volume refers to the steam water added in the bubble absorption bottle.

RH	0%	35%	50%	65%	80%
Flow (mL/min)	4000	4000	4600	4500	5500
Water volume (mL)	0	10	10	27	125

2.4. Sensors and Reference Instrument Detect in Ambient Air

For a comparison of sensors in ambient air, the CO_2 device was housed near the sampling outlet of a reference instrument located approximately 15 m above the laboratory roof. A Picarro (G2401, Picarro Corporation, Santa Clara, CA, USA) was used as the reference instrument for CO_2 concentration comparison. The pipe from the gas inlet to the Picarro was too long to account for a time lag between the ambient air and the instrument reading. To reduce the delay time of the instrument measurements, two circuits were split from the inlet. The by-pass circuit consisted of a flow meter and an auxiliary pump while the other circuit was connected directly to the instrument with a filter.

To evaluate the real-world applicability of the lab-derived correction factors and sensor performance, the sensors were deployed for ambient air CO_2 concentration monitoring alongside the reference instrument during a 7-day monitoring exercise (from 30 August to 6 September 2022). The sampling site was the campus of Zhejiang University of Technology, China. Sensor data and reference instrument data were averaged to 1 h intervals and evaluated over the 7-day period.

The average mixing ratio of atmospheric CO_2 in ambient air measured during the whole campaign period by the reference methods was 439 ± 13 ppm (average ± SD). The minute-averaged temperature and the relative humidity in the sampled air were 24 ± 2.5 °C (average ± SD) and 83 ± 12% (average ± SD) during the field campaign.

3. Results and Discussion

3.1. RH Effects

Humidity and temperature are the key factors affecting the detection performance of optical sensors [27,30]. According to the CO_2 sensor datasheet, a temperature compensation function was applied to this product [31]. Therefore, the environmental interference of the CO_2 sensor was only investigated for humidity in this study. The CO_2 concentration of each sensor when exposed to zero air in the presence of varying RH is shown in Figure 2. Obviously, the measured concentration by the six CO_2 sensors changed to varying degrees as the humidity changed, which was not constant. This is significant since several approaches for the field calibration of sensors have proposed bootstrapping ambient sensor measurements to either nearby reference instruments or the sensor ensemble, but such an approach must assume a constant zero value to deliver a calibration slope [32]. The response of the six CO_2 sensors to zero gas at the same humidity gradient varied in peak value and magnitude, with the peak value of sensor 6# being significantly lower than the other sensors at only 450 ppm and the maximum variation of sensor 4# at about 155 ppm. This means that the individual differences between sensors are considerable even if the sensors are made by the same company.

As sensors 1#, 2# and 6# showed, CO_2 concentration slowly increased within 5 ppm as humidity increased from 35% to 50%. Meanwhile, the other sensors showed a decreasing trend, with the largest decrease of 40 ppm in sensor 4#. A similar phenomenon was found when the humidity increased from 65% to 80% showing an increasing trend except for the decrease in CO_2 concentration in sensor 1#. This demonstrates that the drift of the signal due to humidity interferences varies significantly from a single sensor even for the same series of sensors. It means that measuring the CO_2 concentration using a fixed calibration equation can lead to large errors. We noticed a rapid increase in all sensors when the humidity increased from 0 to 35% and a rapid decrease when the humidity increased from

50% to 65%. In the ambient atmosphere, such rapid changes in RH would not often occur, but this rate of change could well be experienced if a sensor was carried on a person from outdoors to in, or vice versa.

3.2. Correction with RH

Gas concentration is positively related to the voltage signal according to the NDIR sensor detection principle. In order to optimize the sensor detection accuracy, several calibration curves (Figure 3) were fitted to CO_2 standard gas using a gas dilution device with three concentration gradients (400, 600 and 800 ppm) at different humidity conditions. The simulation results for different humidity conditions were calculated based on the slope between voltage values and corresponding concentration values. The signals of the six CO_2 sensors showed a positive correlation with the standard gas concentration, meaning that the linear relationship of the NDIR sensor between gas concentration and voltage does not change as RH varies. The sensitivity of sensor 2# was lower than that of the other sensors, especially at the 600 and 800 ppm, where changes in humidity caused less change in concentration. This is not consistent with the results from the other sensors, which again confirms that individual errors in the sensors can affect the detection results. The same results from the six sensors measured showed that the calibration curves at RH between 35% and 50% were very close and the discrepancy increased when increasing from 50% to 65%. This may indicate that the optimum RH condition for application of the CO_2 sensor is around 50%.

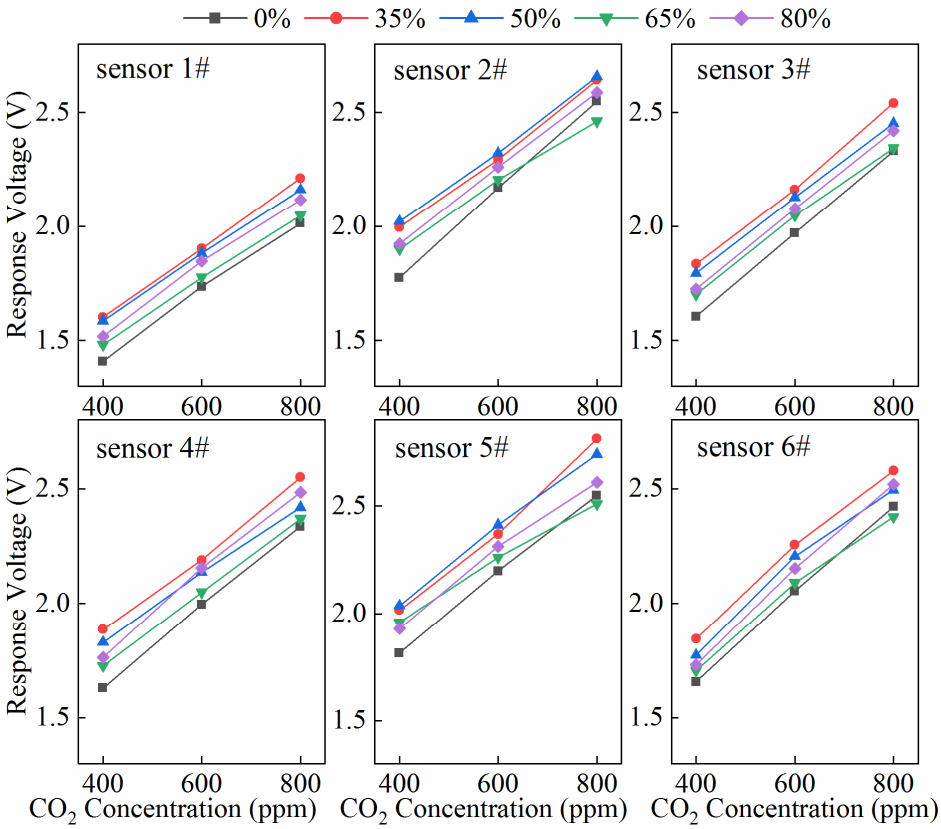

Figure 3. The NDIR CO_2 sensor sensitivity to CO_2 standard gas with 400, 600 and 800 ppm on different RHs of 0%, 35%, 50%, 65% and 80%.

CO_2 concentration in ambient atmosphere is around 400 ppm [33], so we corrected the sensors for humidity interference based on a 400 ppm calibration curve. The CO_2 sensor response is a function of gas concentration and RH of the medium [34]. Therefore, moderating the effect of environmental parameters can improve the reliability of the CO_2

sensor. A regression function defined in Equation (1) corrects the concentration by RH and enhancement value (Δ CO_2 concentration):

$$C_{corrected} = C_{raw} + C_{interference} = C_{raw} + f\ (\text{RH}, \Delta\ CO_2\ \text{concentration}) \quad (1)$$

where $C_{corrected}$ represents the concentration of CO_2 after humdity correction, C_{raw} means the concentration of CO_2 detected directly by the sensors, $C_{interference}$ represents the variation of CO_2 concentration due to humdity and f (RH, Δ CO_2 concentration) denotes a function between RH and CO_2 enhancement value.

The relationship between RH and varying values of CO_2 concentration is shown in Figure 4. The two display a quadratic relationship whose equation and R^2 markers feature in red in the diagram. The results of the fitted curve showed a gradual decrease in Δ CO_2 concentration with increasing RH, with the smallest increment of Δ CO_2 concentration being around 3 ppm around 50% RH, followed by an increase in deviation, reaching a maximum around 65% RH and then decreasing again beyond 65%. The results of the sensors were similar, with R^2 above 0.94 showing a strong correlation. Among the sensors, sensors 1#, 4# and 5# had the best R^2 (of 0.99 or more).

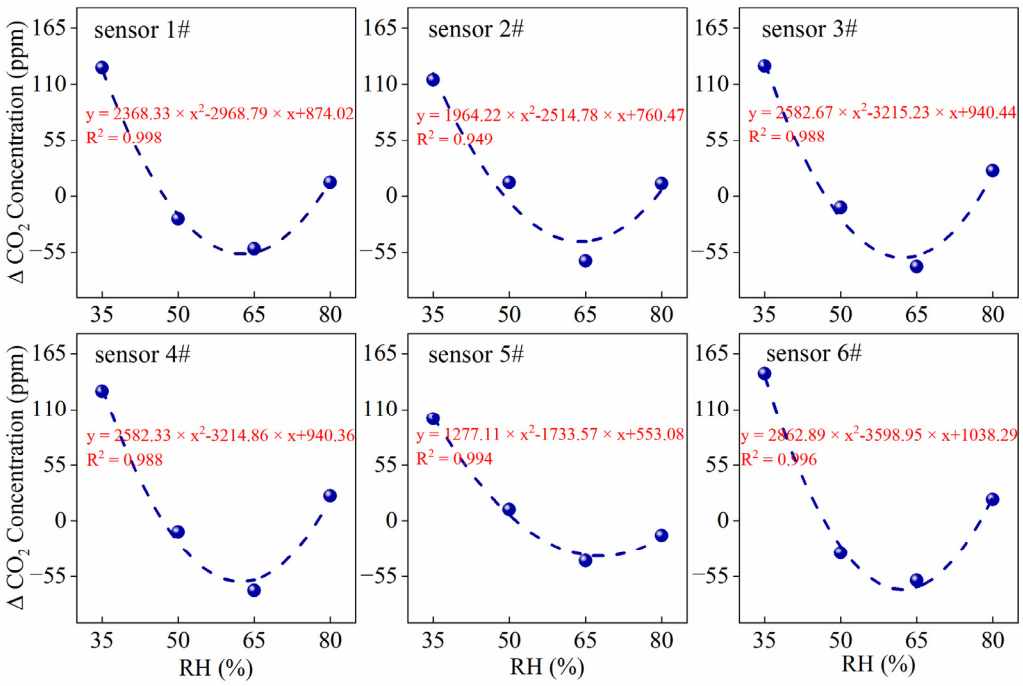

Figure 4. Unitary regression analysis of the varied CO_2 concentration and RH detected by six NDIR CO_2 sensors mounted on the self-developed CO_2 device at laboratory. The regression equation and R^2 are shown above the curves with red, respectively.

RH and temperature was measured by the humidity and temperature sensors integrated into the CO_2 device during the comparison experiment. The results are shown in Figure 5 for the calibration of CO_2 measurements in ambient air. Correction values for CO_2 were obtained by taking the RH measured from outdoor air into the equation measured in the simulation and adding the corresponding humidity interference values to initial measured CO_2 concentration.

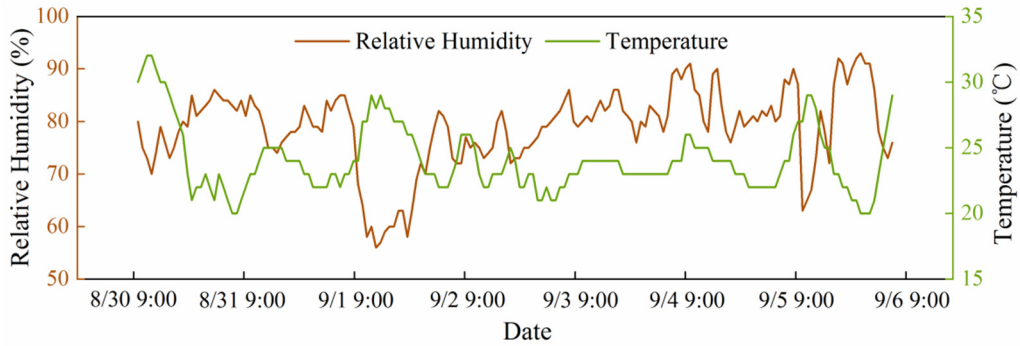

Figure 5. Measured variations of temperatures and RH in ambient air during the field campaign from 30 August 2022–9 September 2022.

3.3. Comparison with Reference Instrument

The results of original measured and humidity corrected values of the CO_2 device compared with the Picarro are shown on the left of Figure 6. During the 7-day period, the Picarro observed variations in ambient CO_2 with a mean value of just above 439 ppm and a standard deviation of just below 14 ppm. There was a clear synoptic variation in the diurnal cycle observed, varying in magnitude from as low as 10 ppm over 24 h to more than 40 ppm. Each of the sensors was successfully able to resolve the ambient variations in CO_2 over this comparison period, although none of the sensors matched the Picarro perfectly in both absolute concentration and relative change. Each individual sensor has a stage to match with the Picarro from Figure 6. A few of the sensors were approximately the same as the Picarro, but many can have an offset that was as much as 6% (25 ppm) from the Picarro. The differences between each sensor and the Picarro all had relative deviations between 4% and 7% (Table 2).

The measured value of the sensor maintained the same trend as the reference instrument after calibration, with a deviation of less than 3% (Table 2). The difference in measurement occurred mainly in the peaks or troughs, which may be due to the difference in response time. The Picarro detection is based on the CRDS method, a technique characterized by a short response time. In contrast, the NDIR method is used for the CO_2 sensor and the sample takes 2 s from diffusion to full detection. The errors caused by the differences in measurement principle become more obvious when exposed to fluctuating CO_2 concentrations. This means that monitoring using CRDS technology are more suitable for studying sudden changes in CO_2, while for some continuous observation experiments inexpensive CO_2 sensors can replace these monitoring. The smallest differences of the six CO_2 sensors before and after calibration were found during the first three and last two days of the field observation experiment. The deviation of sensors 1#, 2#, 3# and 6# increased by approximately 20 ppm while sensors 4# and 5# did not change significantly from 10:00 a.m. on 1 September to 09:00 a.m. on 3 September. However the ambient air humidity shows a dramatic change at this time from 60% to 80% in Figure 5. It is possible that sensors 4# and 5# are not too sensitive at this RH range.

Table 2. Maximum relative deviation of the CO_2 sensors combinations compared with Picarro before and after correction during a 7-day field experiment.

Number of Sensors	1#	2#	3#	4#	5#	6#
Relative deviation (before correction)	6.12%	6.38%	6.91%	5.11%	4.84%	4.25%
Relative deviation (after correction)	2.01%	3.37%	2.46%	1.89%	3.27%	3.45%

The scatter plot and linear fit curves between before and after calibration with the Picarro are shown on the right of Figure 6. The correlation coefficients are located on

both sides of the curves. The correlations of the raw CO_2 data with the Picarro data were improved with calibration by a range of 0.6–0.75. Sensors 1#, 2#, 4# and 6# all had strong correlations with the Picarro above 0.9 after calibration. The R^2 for sensors 3# and 5# was close to around 0.83, which was lower than the other sensors. This indicates that the accuracy of CO_2 has all improved after correction for humidity interferences. Some of the sensors have better detection performance, but there is still measurement error due to individual differences between sensors and this error may be more pronounced.

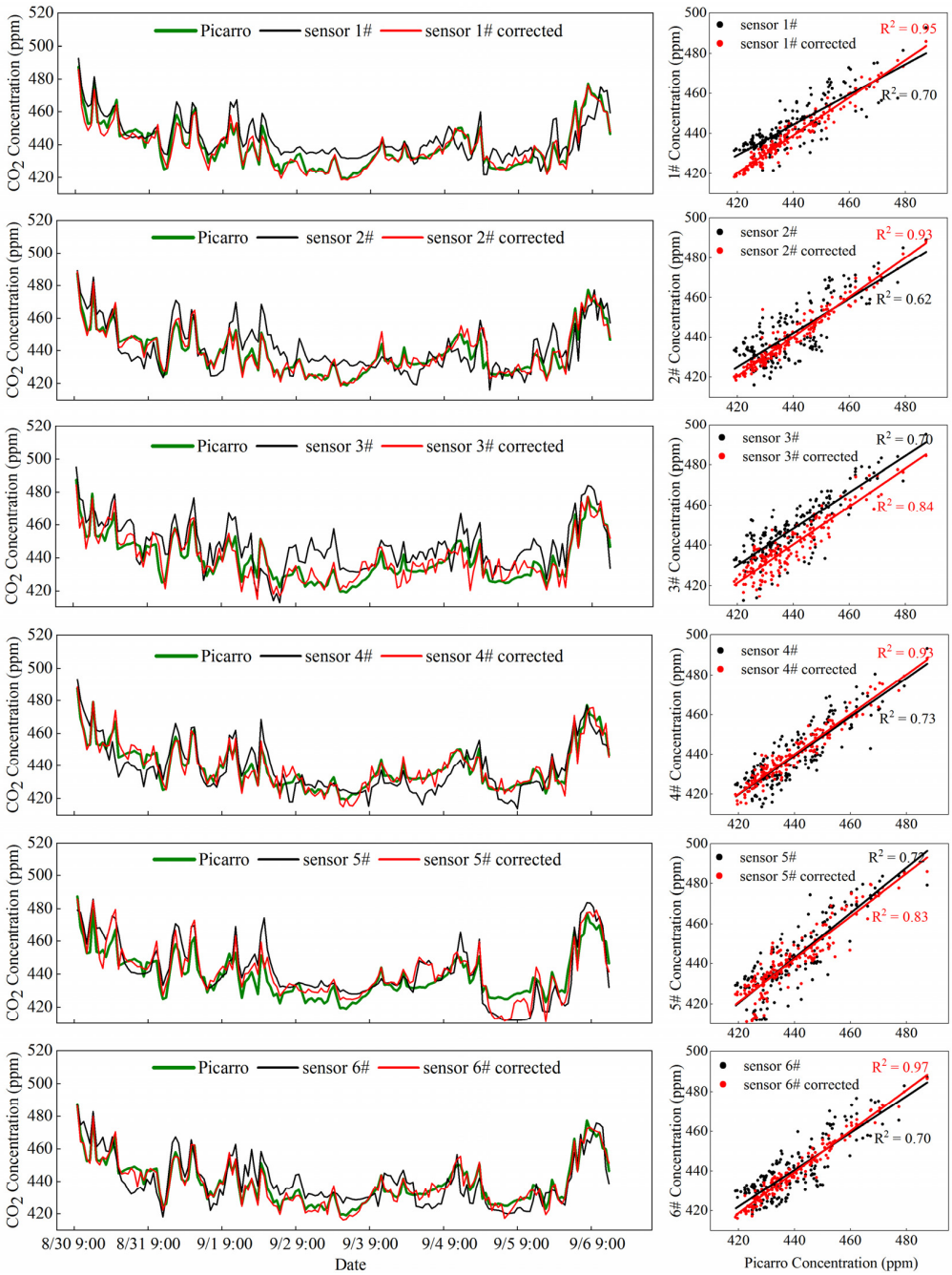

Figure 6. Comparisons between the six CO_2 sensors (one-hour average) and Picarro (one-hour average) during the 7-day field campaign in Hangzhou. The scatter plots representing the correlation relationship between corrected sensor data and Picarro data. The linear regression curves and correlation coefficients are shown as well in the scatter plots.

3.4. Improving Performance by Clustering Sensors

A cluster analysis of the measurement data from six sensors was conducted in order to reduce the influence of individual differences between sensors in the experimental results. At first the relative deviations between each sensor and the reference instrument after calibration were calculated and then the average values were calculated for the sensors according to the permutations in Figure 7. With an increased number of sensors the average relative deviation decreases to a minimum of 1.4%, as shown in Figure 7. The average relative deviation between the sensor and the Picarro after calibration was one third of that before calibration, slightly less than 2%. As the number of sensors in a cluster is increased, the observed range of values for the unique permutations of the groups narrows considerably, greatly improving measurement precision. The relative deviation increased slightly when selecting four sensors compared to selecting three sensors but was still better than using one or two sensors. It is worth noting that if only a single sensor was analyzed, one or several sensors had better deviations than the clustered results. Of course we cannot deny the possibility that the best sensor (close to true value) can be directly selected for environmental monitoring or scientific research, but the probability of this is small. Several studies have shown that clustering analysis using several sensors was a potential technical approach to reduce the effects of drift in individual sensor responses and limiting the effects of manufacturing variability among sensors [35,36]. Therefore a combination of several sensors is a more efficient way to improve the measurement accuracy.

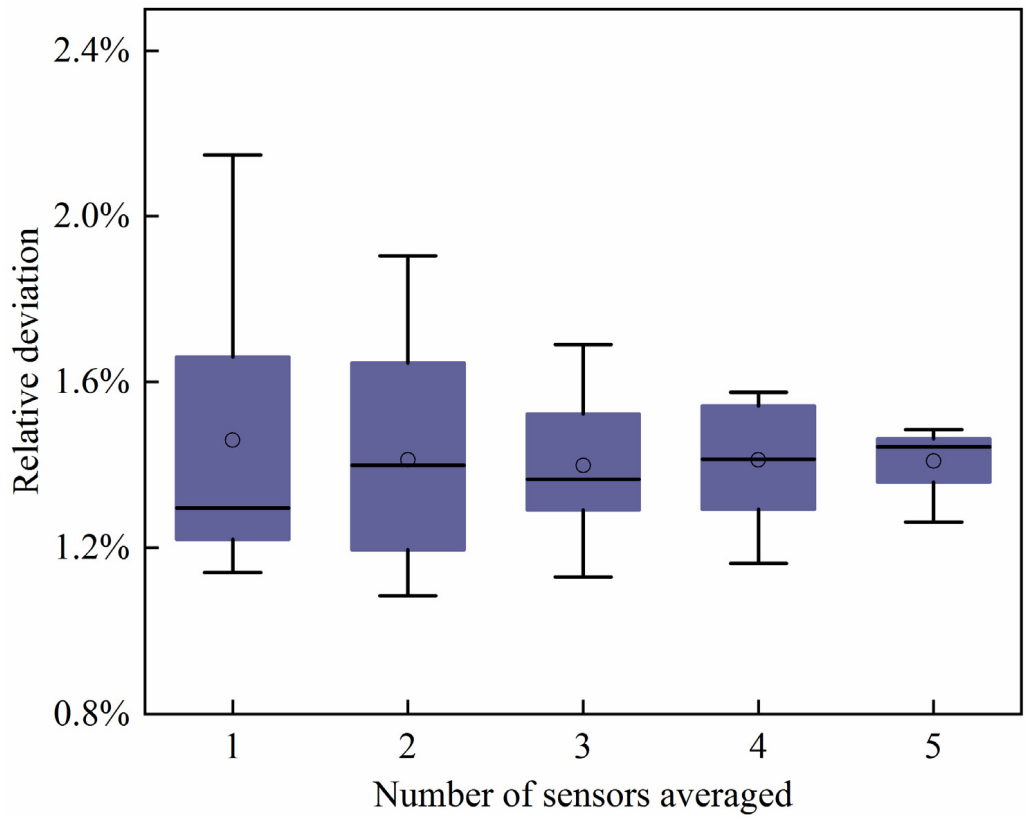

Figure 7. Average relative deviation of the CO_2 sensors combinations compared with the Picarro after RH correction during a 7-day field experiment. The number of sensors means that if data from three out of six sensors are used there are 20 possible permutations of sensors. The 20 gradients of these correlation plots are then plotted in the box plots above, with the median, 25th percentile and 75th percentile in the box and the 5th and 95th percentile on the whiskers.

4. Conclusions

Using a combination of clustering CO_2 sensors with NDIR technology, a portable and highly sensitive CO_2 device was developed for ambient air measurement. The concentration drift of sensors influenced by RH was simulated by a humidity generation unit at a laboratory. A quadratic equation was found between the value of CO_2 concentration variation and RH by regression analysis, with a better correlation range from 0.949 to 0.998. Using the equation it was possible to recreate reference measurements reasonably well when the sensors were tested side-by-side over a 7-day field experiment. The relative deviation of the sensors and the Picarro decreased from 6.91% (a minimum of 4.25%) to 3.45% (a minimum of 1.89%) after calibration. The averaged relative deviation between the clustering sensors and the Picarro gradually decreased as the number of sensors increased. Clustering of sensors adds little to the overall power budget of an instrument but is a very easy way to overcome individual sensor drift and irreproducibility. In general commercial low-cost sensors calibrated with environmental interference are suitable for a variety of scientific applications.

Author Contributions: Z.W.: Conceptualization, Data curation, Software, Writing—original draft preparation, Writing—review and editing. X.P.: Conceptualization, Writing—review and editing, Funding acquisition, Supervision, Project administration. B.X.: Project administration, Investigation, Writing—review and editing. Q.S.: Investigation and data curation. H.W. (Hai Wu): Writing—review and editing, Supervision. Y.L. (Yu Lu): Sofeware and investigaton. H.W. (Haonan Wu): Data curation. Y.L. (Yan Lyu): Data curation. J.L.: Project administration. B.W.: Investigation and data curation. S.D.: Investigation and data curation. D.C.: Investigation and data curation. J.C.: Project administration and Funding acquisition. All authors have read and agreed to the published version of the manuscript.

Funding: This work was supported by National Key R&D Program of China (2022YFC3703500), National Natural Science Foundation of China (41727805), Zhejiang Province "Lingyan" Research and Development Project (2022C03073), Key Research Program of Zhejiang Province (2021C03165), the Natural Science Foundation of Zhejiang Province, China (LZ20D050002), Shaoxing Science and Technology Plan Project (2022B41006), Key project of Scientific and Technological Research Program of Chongqing Municipal Education Commission (KJZD-M202201402 & KJZD-K201901403) and General project of Natural Science Foundation of Chongqing Bureau of science and technology (cstc2019jcyj-msxmX0879 & cstc2019jcyj-msxmX0872).

Institutional Review Board Statement: The study did not require ethical approval.

Informed Consent Statement: The study did not involve humans.

Data Availability Statement: The study did not report any data.

Conflicts of Interest: The authors declare no conflict of interest.

References

1. Ebi, K.L.; Boyer, C.; Ogden, N.; Paz, S.; Berry, P.; Campbell-Lendrum, D.; Hess, J.J.; Woodward, A. Burning embers: Synthesis of the health risks of climate change. *Environ. Res. Lett.* **2021**, *16*, 044042. [CrossRef]
2. Henninger, S.; Kuttler, W. Methodology for mobile measurements of carbon dioxide within the urban canopy layer. *Clim. Res.* **2007**, *34*, 161–167. [CrossRef]
3. Babenhauserheide, A.; Hase, F.; Morino, I. Net CO_2 fossil fuel emissions of Tokyo estimated directly from measurements of the Tsukuba TCCON site and radiosondes. *Atmos. Meas. Technol.* **2020**, *13*, 2697–2710. [CrossRef]
4. Gemery, P.A.; Trolier, M.; White, J.W.C. Oxygen isotope exchange between carbon dioxide and water following atmospheric sampling using glass flasks. *J. Geophys. Res. Atmos.* **1996**, *101*, 14415–14420. [CrossRef]
5. Green, O.; Finkelstein, P.; Rivero-Crespo, M.A.; Lutz, M.D.R.; Bogdos, M.K.; Burger, M.; Leroux, J.C.; Morandi, B. Activity-Based Approach for Selective Molecular CO_2 Sensing. *J. Am. Chem. Soc.* **2022**, *144*, 8717–8724. [CrossRef]
6. Morozov, O.; Tunakova, Y.; Hussein, S.; Shagidullin, A.; Agliullin, T.; Kuznetsov, A.; Valeev, B.; Lipatnikov, K.; Anfinogentov, V.; Sakhabutdinov, A. Addressed Combined Fiber-Optic Sensors as Key Element of Multisensor Greenhouse Gas Monitoring Systems. *Sensors* **2022**, *22*, 4827. [CrossRef]

7. Buchwitz, M.; Reuter, M.; Noel, S.; Bramstedt, K.; Schneising, O.; Hilker, M.; Andrade, B.F.; Bovensmann, H.; Burrows, J.P.; Di Noia, A.; et al. Can a regional-scale reduction of atmospheric CO_2 during the COVID-19 pandemic be detected from space? A case study for East China using satellite XCO2 retrievals. *Atmos. Meas. Technol.* **2021**, *14*, 2141–2166. [CrossRef]
8. Miller, S.M.; Michalak, A.M. The impact of improved satellite retrievals on estimates of biospheric carbon balance. *Atmos. Chem. Phys.* **2020**, *20*, 323–331. [CrossRef]
9. Zheng, B.; Chevallier, F.; Ciais, P.; Broquet, G.; Wang, Y.L.; Lian, J.H.; Zhao, Y.H. Observing carbon dioxide emissions over China's cities and industrial areas with the Orbiting Carbon Observatory-2. *Atmos. Chem. Phys.* **2020**, *20*, 8501–8510. [CrossRef]
10. Lee, H.; Han, S.O.; Ryoo, S.B.; Lee, J.S.; Lee, G.W. The measurement of atmospheric CO_2 at KMA GAW regional stations, its characteristics, and comparisons with other East Asian sites. *Atmos. Chem. Phys.* **2019**, *19*, 2149–2163. [CrossRef]
11. Li, Z.B.; Ma, H.L.; Cao, Z.S.; Sun, M.G.; Huang, Y.B.; Zhu, W.Y.; Liu, Q. High-sensitive off-axis integrated cavity output spectroscopy and its measurement of ambient CO_2 at 2 μm. *Acta Phys. Sin.* **2016**, *65*, 053301.
12. Xin, F.X.; Li, J.; Guo, J.J.; Yang, D.W.; Wang, Y.; Tang, Q.H.; Liu, Z.S. Measurement of Atmospheric CO_2 Column Concentrations Based on Open-Path TDLAS. *Sensors* **2021**, *21*, 1722. [CrossRef] [PubMed]
13. Chandra, N.; Patra, P.K.; Niwa, Y.; Ito, A.; Iida, Y.; Goto, D.; Morimoto, S.; Kondo, M.; Takigawa, M.; Hajima, T.; et al. Estimated regional CO_2 flux and uncertainty based on an ensemale of atmospheric CO_2 inversions. *Atmos. Chem. Phys.* **2022**, *22*, 9215–9243. [CrossRef]
14. Huang, B.B.; Lu, F.; Wang, X.K.; Wu, X.; Zhang, L.; Ouyang, Z.Y. Ecological restoration and rising CO_2 enhance the carbon sink, counteracting climate change in northeastern China. *Environ. Res. Lett.* **2022**, *17*, 014002. [CrossRef]
15. Paris, J.D.; Riandet, A.; Bourtsoukidis, E.; Delmotte, M.; Berchet, A.; Williams, J.; Ernle, L.; Tadic, I.; Harder, H.; Lelieveld, J. Shipborne measurements of methane and carbon dioxide in the Middle East and Mediterranean areas and the contribution from oil and gas emissions. *Atmos. Chem. Phys.* **2021**, *21*, 12443–12462. [CrossRef]
16. Yue, X.; Liao, H.; Wang, H.J.; Zhang, T.Y.; Unger, N.; Sitch, S.; Feng, Z.Z.; Yang, J. Pathway dependence of ecosystem responses in China to 1.5 degrees C global warming. *Atmos. Chem. Phys.* **2020**, *20*, 2353–2366. [CrossRef]
17. Struzik, M.; Garbayo, I.; Pfenninger, R.; Rupp, J.L.M. A Simple and Fast Electrochemical CO_2 Sensor Based on $Li_7La_3Zr_2O_{12}$ for Environmental Monitoring. *Adv. Mater.* **2018**, *30*, 1804098. [CrossRef]
18. Aono, H.; Sadaoka, Y.; Montanaro, L.; Di Bartolomeo, E.; Traversa, E. Humidity influence on the CO_2 response of potentiometric sensors based on NASICON pellets with new compositions, $Na_3Zr_{2-(x/4)}Si_{2-x}P_{1+x}O_{12}$(x=1.333). *J. Am. Ceram. Soc.* **2002**, *85*, 585–589. [CrossRef]
19. Obata, K.; Kumazawa, S.; Shimanoe, K.; Miura, N.; Yamazoe, N. Potentiometric sensor based on NASICON and In_2O_3 for detection of CO_2 at room temperature-modification with foreign substances. *Sens. Actuators B* **2001**, *76*, 639–643. [CrossRef]
20. Vafaei, M.; Amini, A.; Siadatan, A. Breakthrough in CO_2 Measurement With a Chamberless NDIR Optical Gas Sensor. *IEEE Trans. Instrum. Meas.* **2020**, *69*, 2258–2268. [CrossRef]
21. Tan, X.; Zhang, H.; Li, J.; Wan, H.; Guo, Q.; Zhu, H.; Liu, H.; Yi, F. Non-dispersive infrared multi-gas sensing via nanoantenna integrated narrowband detectors. *Nat. Commun.* **2020**, *11*, 5245. [CrossRef] [PubMed]
22. Jia, X.; Roels, J.; Baets, R.; Roelkens, G. On-Chip Non-Dispersive Infrared CO_2 Sensor Based on an Integrating Cylinder. *Sensors* **2019**, *19*, 4260. [CrossRef]
23. De Azevedo, G.B.H.; Doyle, B.; Fiebrich, C.A.; Schvartzman, D. Low-complexity methods to mitigate the impact of environmental variables on low-cost UAS-based atmospheric carbon dioxide measurements. *Atmos. Meas. Technol.* **2022**, *15*, 5599–5618. [CrossRef]
24. Vincent, T.A.; Gardner, J.W. A low cost MEMS based NDIR system for the monitoring of carbon dioxide in breath analysis at ppm levels. *Sens. Actuators B* **2016**, *236*, 954–964. [CrossRef]
25. Han, J.H.; Han, S.W.; Kim, S.M.; Pak, J.J.; Moon, S. High Detection Performance of NDIR CO_2 Sensor Using Stair-Tapered Reflector. *IEEE Sens. J.* **2013**, *13*, 3090–3097. [CrossRef]
26. Hussain, H.; Kim, J.; Yi, S. Characteristics and Temperature Compensation of Non-Dispersive Infrared (NDIR) Alcohol Gas Sensors According to Incident Light Intensity. *Sensors* **2018**, *18*, 2911. [CrossRef]
27. Dinh, T.V.; Choi, I.Y.; Son, Y.S.; Kim, J.C. A review on non-dispersive infrared gas sensors: Improvement of sensor detection limit and interference correction. *Sens. Actuators B* **2016**, *231*, 529–538. [CrossRef]
28. Jia, X.; Roels, J.; Baets, R.; Roelkens, G. A Miniaturised, Fully Integrated NDIR CO_2 Sensor On-Chip. *Sensors* **2021**, *21*, 5347. [CrossRef] [PubMed]
29. Arzoumanian, E.; Vogel, F.R.; Bastos, A.; Gaynullin, B.; Laurent, O.; Ramonet, M.; Ciais, P. Characterization of a commercial lower-cost medium-precision non-dispersive infrared sensor for atmospheric CO_2 monitoring in urban areas. *Atmos. Meas. Technol.* **2019**, *12*, 2665–2677. [CrossRef]
30. Joe, H.E.; Yun, H.; Jo, S.H.; Jun, M.B.G.; Min, B.K. A Review on Optical Fiber Sensors for Environmental Monitoring. *Int. J. Precis. Eng. Manuf. Green Technol.* **2018**, *5*, 173–191. [CrossRef]
31. K30 10,000ppm CO2 Sensor. Available online: https://www.co2meter.com/products/k-30-co2-sensor-module (accessed on 14 December 2022).
32. Pang, X.; Shaw, M.D.; Gillot, S.; Lewis, A.C. The impacts of water vapour and co-pollutants on the performance of electrochemical gas sensors used for air quality monitoring. *Sens. Actuators B* **2018**, *266*, 674–684. [CrossRef]

33. Chaterjee, S.; Krupadam, R.J. Amino acid-imprinted polymers as highly selective CO_2 capture materials. *Environ. Chem. Lett.* **2019**, *17*, 465–472. [CrossRef]
34. Vafaei, M.; Amini, A. Chamberless NDIR CO_2 Sensor Robust against Environmental Fluctuations. *ACS Sens.* **2021**, *6*, 1536–1542. [CrossRef] [PubMed]
35. Smith, K.R.; Edwards, P.M.; Evans, M.J.; Lee, J.D.; Shaw, M.D.; Squires, F.; Wilde, S.; Lewis, A.C. Clustering approaches to improve the performance of low cost air pollution sensors. *Faraday Discuss.* **2017**, *200*, 621–637. [CrossRef]
36. Smith, K.R.; Edwards, P.M.; Ivatt, P.D.; Lee, J.D.; Squires, F.; Dai, C.L.; Peltier, R.E.; Evans, M.J.; Sun, Y.L.; Lewis, A.C. An improved low-power measurement of ambient NO_2 and O_3 combining electrochemical sensor clusters and machine learning. *Atmos. Meas. Technol.* **2019**, *12*, 1325–1336. [CrossRef]